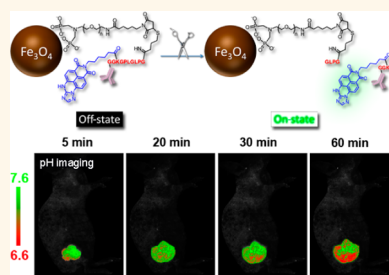


Protease-Activated Ratiometric Fluorescent Probe for pH Mapping of Malignant Tumors

Yi Hou,[†] Jin Zhou,[†] Zhenyu Gao,^{†,*} Xiaoyu Sun,[†] Chunyan Liu,[†] Dihua Shangguan,[†] Wensheng Yang,[‡] and Mingyuan Gao^{*,†}

[†]Institute of Chemistry, Chinese Academy of Sciences, Bei Yi Jie 2, Zhong Guan Cun, Beijing 100190, China and [‡]College of Chemistry, Jilin University, Changchun 130012, China

ABSTRACT A protease-activated ratiometric fluorescent probe based on fluorescence resonance energy transfer between a pH-sensitive fluorescent dye and biocompatible Fe₃O₄ nanocrystals was constructed. A peptide substrate of MMP-9 served as a linker between the particle quencher and the chromophore that was covalently attached to the antitumor antibody. The optical response of the probe to activated MMP-9 and gastric cell line SGC7901 tumor cells was investigated, followed by *in vivo* tumor imaging. Based on the ratiometric pH response to the tumor microenvironment, the resulting probe was successfully used to image the pH of subcutaneous tumor xenografts.



KEYWORDS: Fe₃O₄ nanocrystals · protease-activated · pH mapping · ratiometric fluorescence · smart probe

It is well-known that the tumor microenvironment is strongly correlated with prognostic factors relating to growth, invasion, and metastasis of malignant tumors.^{1–9} Furthermore, there is increasing awareness of the impact of spatiotemporal heterogeneity in tumor properties that impact therapeutic administration. Therefore, developing noninvasive methods for visualizing the tumor microenvironment is critical for tumor diagnostics and for predicting metastasis potential, determining therapeutic efficacy, therapy development, and prognostics. In a clinical scenario, this information could also direct personalized care specified by the tumor response.

Tumor cells need to breach extracellular matrices to invade. Conventionally, matrix metalloproteases (MMPs), a family of zinc-dependent secreted endopeptidases, are involved in homeostatic regulation and processing of extracellular matrices.² However, their overexpression observed in tumors compromises extracellular matrix integrity and correlates with an advanced tumor stage, increased invasion and metastasis, and shortened survival.^{4–7} Normally, MMPs occur in unactivated zymogen form, whereas they are activated and upregulated in almost all types of human cancers.

Apart from abnormal expression of proteases, the tumor microenvironment is also often characterized by abnormal extracellular pH as a result of anaerobic glycolysis, typically in a range of 6.2–6.9 and slightly lower than that (7.2–7.4) for normal tissues.³ The acidic environment of malignant tumors correlates with a significant number of harmful consequences, such as increased invasion and mutation rates as well as and radio resistance.^{8,9} Monitoring the MMP activity and pH in tumors is therefore of major significance in the study and treatment of cancer.

Various optical imaging labels have been developed as facile and hypersensitive tools for biosensing, yet they often suffer *in vivo* from the interference of autofluorescence.¹⁰ One solution to reduce the background noise arising from autofluorescence is to quench the fluorescence of the probes before reaching the designated target. If the fluorescence can be activated at the target site, by endogenous enzymes for example, hypersensitive and enzyme-specific fluorescent probes can be realized.^{11–16}

Inorganic nanoparticles such as Au particles are often chosen as a quencher for constructing hypersensitive optical probes based on fluorescence resonance energy

* Address correspondence to gaomy@iccas.ac.cn.

Received for review January 13, 2015 and accepted February 10, 2015.

Published online February 11, 2015
10.1021/acsnano.5b00276

© 2015 American Chemical Society

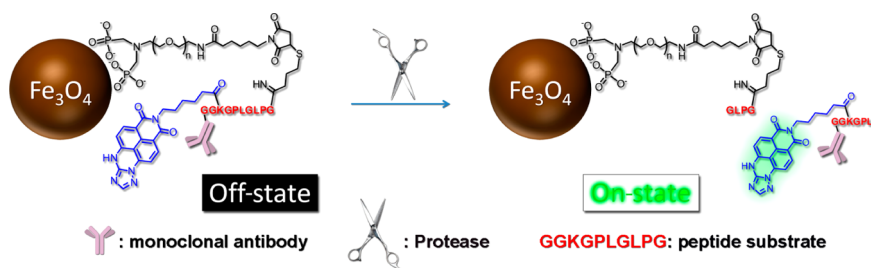


Figure 1. Transition from “off-state” to “on-state” of the fluorescent probe can be triggered by MMP-9.

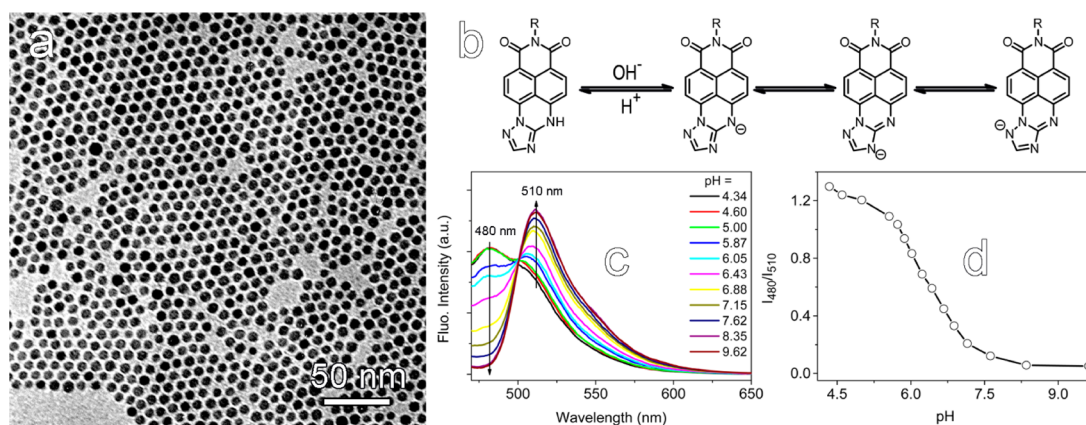


Figure 2. TEM image of the as-prepared Fe_3O_4 nanoparticles (a), protonation/deprotonation induced structural transformation of ANNA (b), pH-dependent fluorescence of ANNA recorded under excitation of 455 nm (c), and ratiometric fluorescence behavior of ANNA against pH (d).

transfer (FRET).¹⁵ In comparison with Au particles, iron oxide nanocrystals exhibit broad featureless absorption in the visible domain due to the electronic transition of d-orbitals.^{17,18} Therefore, magnetic iron oxide nanoparticles can, in principle, also be used as a quencher for constructing FRET-based target-activated optical probes, which remains to be explored. An additional benefit of using magnetic iron oxide particles instead of Au particles is that they can enhance the local contrast of magnetic resonance imaging.^{19–22}

Regarding pH sensing, most fluorescent probes developed so far solely rely on the variation of fluorescence intensity, which is usually compromised by many non-pH factors such as the local concentration of chromophores.²³ In contrast, ratiometric fluorescent probes can avoid such problem and thus allow quantitative determination of pH.^{23–29}

Herein, we propose a protease-activated fluorescence imaging probe based on Fe_3O_4 nanocrystals and ratiometric fluorescent dye that are covalently linked through a peptide substrate of MMP-9, as depicted in Figure 1. In its “off-state”, the Fe_3O_4 particle is designed to quench the fluorescence of the dye, that is, the *N*-carboxyhexyl derivative of 3-amino-1,2,4-triazole-fused 1,8-naphthalimide (ANNA). When MMP-9 cleaves the peptide linker, the quenching particle is lost and the dye fluoresces, representing the “on-state”. It is worthy to mention that a tumor-specific antibody covalently coupled to the C-terminal

of the peptide substrate remains attached to the chromophore after detachment. This is intended for retaining the chromophores within the tumor extracellular matrix to enable pH mapping. This design makes the current probe significantly different from activatable probes reported before.^{11–15} Through a series of *in vitro* and *in vivo* experiments, the performance of the probe was evaluated. The pH of the tumors *in vivo* was imaged to demonstrate the feasibility of the probe design for tumor microenvironmental analysis.

RESULTS AND DISCUSSION

Construction of Protease-Activated Fluorescent Imaging Probe. The Fe_3O_4 nanocrystals with an average size of 7.2 ± 0.6 nm, as shown in Figure 2a, were prepared through a conventional thermal decomposition method by using oleic acid as surface ligands.³⁰ By using an asymmetric polyethylene glycol (PEG) ligand bearing a diphosphate group at one end and a maleimide group at the other end to displace the hydrophobic ligands, PEGylated Fe_3O_4 nanoparticles were obtained.²² Through the maleimide group, ANNA-labeled peptide (*i.e.*, Gly-Pro-Leu-Gly-Leu-Pro-Gly-Lys-Gly-Gly) was covalently linked to the particle surface.^{31,32} Thereafter, a gastric-cancer-specific anti-gastric cancer antibody MGB_2 was attached to the C-terminal of the peptide substrate through an amidation reaction. MGB_2 is a mouse monoclonal antibody developed by immunizing

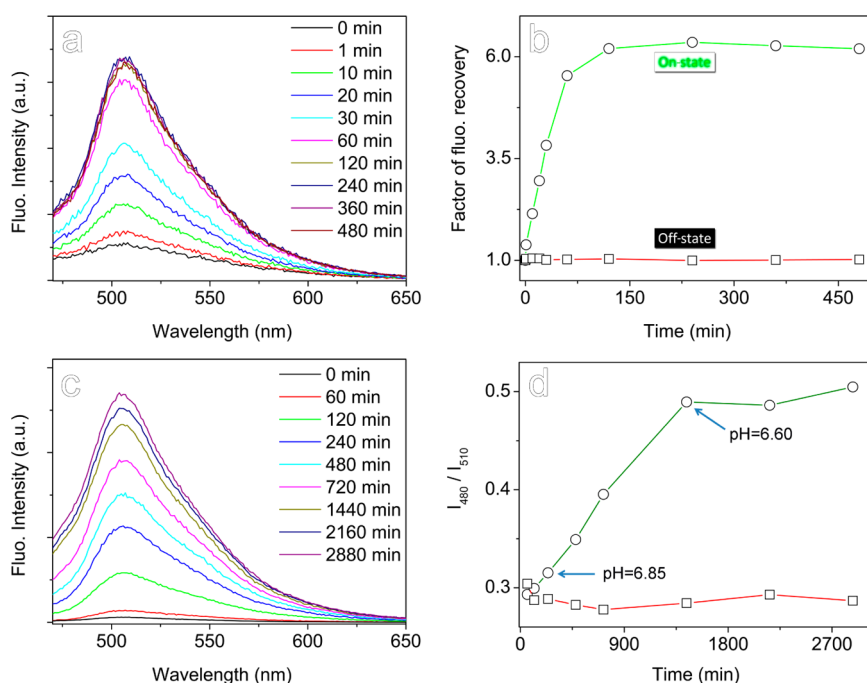


Figure 3. Fluorescence spectra of the probe incubated with the MMP-9 in $1\times$ PBS (a), temporal evolution of fluorescence peak intensity in the presence (green) or absence (red) of MMP-9 (b), fluorescence spectra of the probe incubated with SGC7901 cells (c), and ratiometric fluorescence behaviors recorded in the presence of SGC7901 cells (green) and human fibroblast cells (red) (d).

BALB/c mice with the KATOIII gastric cancer cell line. Its antigen identified as TRAK1 (trafficking protein, kinesin-binding 1) is expressed in 81.48% of gastric carcinomas and 100% of signet ring cell carcinomas, which makes MGB₂ a promising ligand for targeting gastric tumor.³³

Due to the deprotonation and internal charge transfer from the electron-rich amino group to the electron-poor imide moiety, as illustrated in Figure 2b, ANNA presents a strong pH-dependent ratiometric emission, as shown in Figure 2c. The resulting intensity ratio of the fluorescence acquired at 480 and 510 nm (*i.e.*, I_{480}/I_{510}) exhibits a sharp decrease especially in the range of 5.7–7.1 (Figure 2d), which is especially interesting for detecting tumor-associated microenvironmental pH. Most importantly, owing to the rational design, the fluorescence of ANNA is heavily quenched after being conjugated to the surface of Fe₃O₄ nanoparticles, and this quenching effect is almost pH-independent in 5.0–7.4, as shown in Supporting Information Figure S1, presenting the “off-state” of the nanoprobe.

Dynamic light scattering (DLS) measurements revealed that the hydrodynamic size of the final probe was of 42 nm, reasonably larger than that (31 nm) for the PEGylated mother particle. Most importantly, as shown in Figure S2, the size distribution profile of the conjugates remains nearly unchanged in comparison with that of the mother particles, which strongly supports that the sequential conjugation reactions took place in a controlled manner.

Protease-Responsive Fluorescence of the Activatable Nanoprobe. The temporal protease-responsive behavior of the nanoprobe was evaluated in $1\times$ phosphate buffered saline (PBS) (pH = 7.4) containing 15 nM activated MMP-9. As shown in Figure 3a, the initial fluorescence intensity of the conjugate is rather weak but is readily enhanced in the presence of MMP-9 by a factor of >6 within 120 min, as illustrated in Figure 3b. In contrast, the fluorescence intensity of the probe remained nearly unchanged over 8 h in the absence of MMP-9 (off-state), indicating excellent sensitivity to MMP-9.

The cancer cell-responsive behavior of the probe was studied by incubating the final probe with tumor cells overexpressing MMP-9, such as human gastric cancer cell line SGC7901.³⁴ Data shown in Figure 3c clearly reveal that fluorescence is effectively activated by SGC7901 cells. Fluorescence imaging revealed that SGC7901 cells present green-colored fluorescence 6 h after being incubated with the probe, while the human fibroblast control cells do not show any observable fluorescence under the same conditions, as shown in Figure S3, consistent with the expectations for the MMP-9 expressing cells.

According to the temporal evolution of the I_{480}/I_{510} ratio provided in Figure 3d, the local pH for the chromophore remains above 6.85 during the early stage of incubation (<6 h), then it is decreased to approximately 6.60 while the I_{480}/I_{510} ratio enters into a plateau region after 24 h incubation. The lowered pH is probably associated with the lysosomal process following the endocytosis of the fluorescent moiety

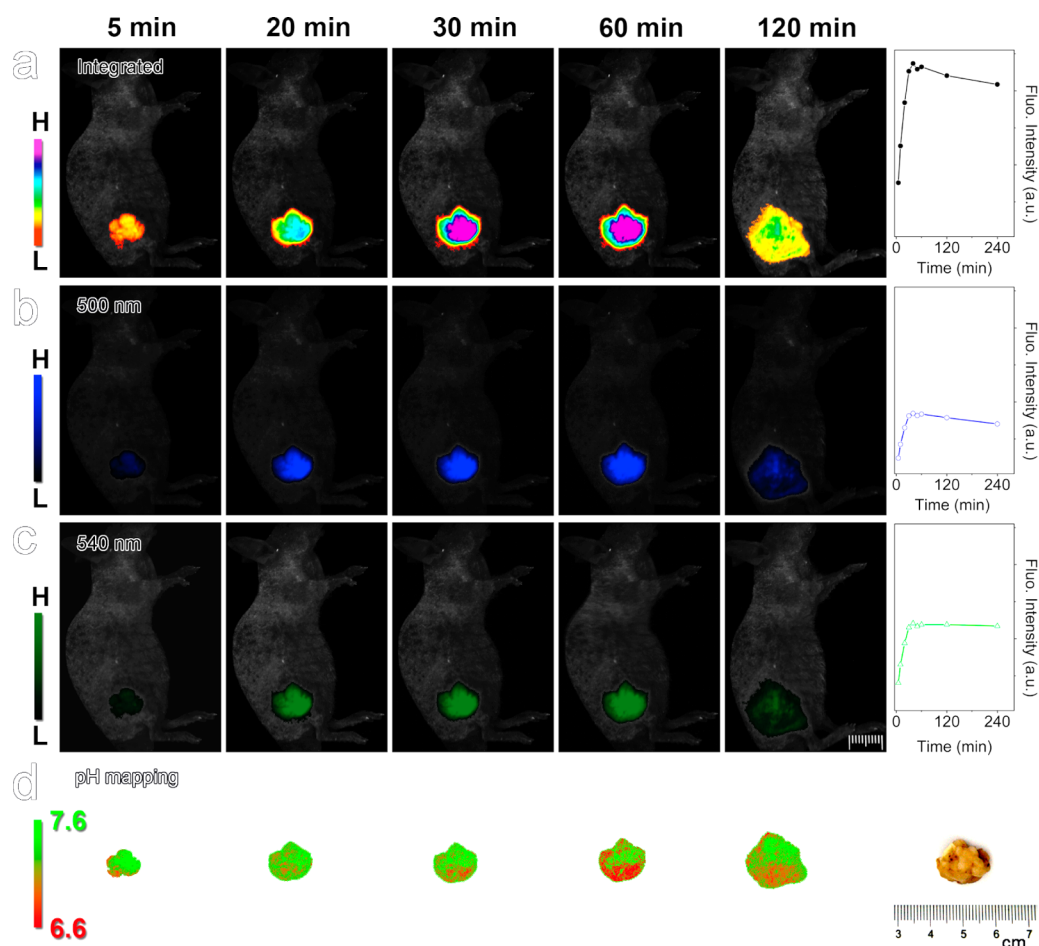


Figure 4. Color-coded fluorescence images of tumor-bearing mice based on emission of 500–600 nm (a), 500 nm (b), and 540 nm (c), with temporal variations of the integrated optical intensity lying aside. Pictures in row d are pH mapping of the tumor region with an optical image of the harvested tumor placed at right-hand side.

remaining attached to the antibody. Nevertheless, roughly 90% of the chromophores remain located on the cell membrane if we assume that the local pH of the lysosome is around 5.0,³⁵ which is greatly in favor of the detection of extracellular pH of tumors in the following *in vivo* studies.

pH Imaging of Tumors *in Vivo*. On the basis of aforementioned results, *in vivo* imaging of the probe in a subcutaneous SGC7901 tumor xenograft was subsequently conducted *via* intratumor injection of the nanoprobe. This was conducted as a proof of principle to demonstrate the feasibility of applications with the probe. As shown in Figure 4a, the fluorescence from the tumor site becomes detectable 5 min post-injection, increases, and then reaches a plateau region between 30 and 60 min. Beyond this time point, the integrated fluorescence intensity slightly decreases. Since the fluorescent area expands in size, the fluorescence intensity of the central tumor area decreases slightly. Since no fluorescence recovery is recorded after subcutaneous injection of the nanoprobe into healthy tissue of normal mice, which served as the control (Figure S4), the appearance and following enhancement of the fluorescence from the tumor

region can be attributed to the probe activation by MMP-9. The latter expansion of the fluorescent area can be interpreted by outward diffusion of the released chromophores that are much smaller than the initial nanoprobe. However, the outward diffusion of the detached dye–antibody conjugate should also be balanced by antibody–target recognition. As a consequence, within a 30 min time window between, the size and shape of the fluorescent area remain nearly unchanged, allowing extraction of the extracellular pH information within tumor.

It should be noted that, due to the limitation of the imaging system used here, fluorescence measurements were restricted only down to 500 nm. Fluorescence at 500 nm (Figure 4b) and 540 nm (Figure 4c) instead of 480 and 510 nm was recorded to extract the pH of the tumor matrix, though with slightly reduced sensitivity (Figure S5a).

Though accurately extracting the pH information solely based the two-dimensional (2D) optical imaging results remains difficult due to the three-dimensional nature and inhomogeneous structure of a given tumor, the absorption and scattering of excitation and emission by both tumor tissue and the overlying skin, etc.,

semiquantitative analysis was carried out by taking the absorption of skin into consideration. More detailed calibration processes on the optical signals are provided in Supporting Information. The corrected I_{500}/I_{540} ratio together with its pH dependency (Figure S5b) then allows pH mapping of the tumor region. We observe here that the pH falls in the range of 6.6–7.5 with an average value of ~ 6.8 for the entire tumor observed 20–60 min postinjection. The detailed results given in Figure 4d further reveal that, during the early stages after administration, the pH imaging contrast remains low but gradually enhances with time. At around 60 min postinjection, the pH inhomogeneity of the entire tumor is maximized. It is worth mentioning that, at this imaging time point, the size of 2D fluorescent image remains rather comparable with that for the tumor extracted right after the imaging experiment (right corner of Figure 4d). Thereafter, the pH imaging contrast is gradually reduced. In fact, the integrated fluorescence intensity only decreases by 5.1% from 1 to 2 h postinjection, but the size of fluorescent area is obviously enlarged. Therefore, the following reduced pH contrast is reasonably attributed to the outward diffusion of the chromophores into healthy tissue, whose pH is typically around 7.4. Assuming that the diffusion takes place isotropically, the chromophores that get closer to skin also contribute to the reduced pH imaging contrast upon prolonged observation.

The fluorescence imaging results indicate that the current probe can rapidly respond to the tumor-associated protease and then sense the extracellular pH of the tumor. Nonetheless, due to the lack of a diffusion coefficient of the dye–antibody conjugate within tumor, the local receptor density, and binding kinetics of the targeting moiety *in vivo*, it remains difficult to disclose the correlation between the

pH imaging and the heterogeneity of the tumor. Moreover, the optical properties of the ratiometric dye can further be optimized for *in vivo* applications by shifting the fluorescence and excitation more to the red. Regarding the current probe design, higher antibody-to-dye ratio is in favor of more accurate tumor pH imaging but is unfavorable for the probe to escape the uptake by the immune system if delivered through intravenous injection. However, the targeting moiety used in the current design is not restricted to the antibody; small targeting molecules may be helpful for further improving the signal-to-noise ratio for the pH mapping. In addition, the core particle of the current protease-activable probe— Fe_3O_4 nanocrystals—also offers the possibility to visualize the heterogeneous structure of tumors *via* magnetic resonance imaging for better understanding of the pH mapping results, which is currently still underway.

CONCLUSIONS

In summary, a protease-activated fluorescent probe is designed and constructed based on FRET between ratiometric fluorescent dye and biocompatible Fe_3O_4 nanocrystals covalently coupled through a MMP-9 specific peptide substrate linker. *In vitro* cell studies prove that the resulting nanoprobe can be activated by MMP-9 secreted by tumor cells. The detached chromophores can effectively tag the tumor cells through the covalently coupled antibody. Further *in vivo* imaging experiments in combination with semiquantitative analysis suggest that the current probe can be used for realizing sensitive pH mapping of the tumor microenvironment. Although a satisfying heterogeneity tumor model is still lacking, the current study paves an effective way to achieve novel probes suitable for noninvasive analysis of tumor-associated microenvironment.

EXPERIMENTAL SECTION

Chemicals. The following materials were purchased from Sigma-Aldrich: $\text{FeCl}_3 \cdot 6\text{H}_2\text{O}$, oleic acid, 1-octadecene, and 4-(4,6-dimethoxy-1,3,5-triazin-2-yl)-4-methylmorpholinium chloride (DMTMM). Analytical grade chemicals such as ethanol, cyclohexane, and tetrahydrofuran (THF) were purchased from Sinopharm Chemical Reagent Beijing, Co., Ltd. The mal-PEG-dp was a customized product provided by Beijing Oneder Hightech Co. Ltd. Human gastric cancer cell line SGC7901 and MGB₂ monoclonal antibody were obtained from the Fourth Military Medical University. Human fibroblast was obtained from the Oncology School of Peking University. Ironoleate complex was prepared according to a previous report.³⁰

Synthesis of Hydrophobic Fe_3O_4 Nanoparticles. Fe_3O_4 nanoparticles with core size of 7.2 nm were also synthesized according to a previous report.³⁰ In brief, 3.6 g (4 mmol) of freshly prepared iron oleate and 3.39 g (4 mmol) of oleic acid were dissolved in 25 mL of 1-octadecene. The resulting solution was heated to 310 °C at a rate of 3.3 °C/min and then maintained at 310 °C for 30 min under nitrogen protection. The preparation was terminated by cooling the reaction mixture to room temperature.

The resulting nanoparticles were precipitated by acetone, collected by magnetic separation, washed with acetone several times, and finally redispersed in THF or cyclohexane for further experiments.

Ligand Exchange. As a typical example, 150 mg of PEG derivative was dissolved in 10 mL of THF containing 10 mg of hydrophobic Fe_3O_4 nanoparticles. Then, the reaction mixture was heated to 60 °C and kept at this temperature for 12 h under stirring. After that, the Fe_3O_4 nanoparticles were precipitated by cyclohexane, washed with cyclohexane three times, and dried under vacuum at room temperature. To remove excess PEG ligand, the resulting aqueous solutions containing the PEGylated Fe_3O_4 nanoparticles were purified by ultrafiltration for 4 cycles using a 100 kDa MWCO centrifugal filter (Millipore YM-100) at 6000 g.

Synthesis of Chromophore-Labeled Peptide. The ratiometric fluorescent dye ANNA was covalently bound with the peptide substrate through an amidation reaction between the carboxyl group of ANNA and the side amino group of Lys in the peptide. In brief, 0.84 mg of ANNA was dissolved in 0.2 mL of 0.01 M PBS (pH 8.5). Then, 0.2 mL of aqueous solution containing 0.6 mg of DMTMM was added quickly under stirring. After 5 min, 0.4 mL

of aqueous solution containing 2 mg of the Boc-protected N-terminal peptide substrate of MMP-9 was added quickly under stirring. The reaction solution was stirred for 1 h. To remove the terminal Boc group, 0.8 mL of trifluoroacetic acid was added. After 1 h, TFA was removed by rotary evaporation. Then, 5 M NaOH was added to the resulting solution, and the pH was adjusted to 6.5. The product was finally obtained for the following synthesis.

Conjugation Reaction between Chromophore-Labeled Peptides and the PEGylated Fe₃O₄ Nanocrystals. To the solution of chromophore-labeled peptide obtained in the previous step was added 0.15 mg of 2-iminothiolane hydrochloride (ca. 1.1 equiv to amino groups). After being stirred for 2 h at room temperature, 2.5 mL of aqueous solution containing 10 mg of (mal-PEG-dp)-coated Fe₃O₄ nanoparticle was added quickly. The mixture was stirred for 1 h, after which the product was purified by ultrafiltration with 1 × PBS for 4 cycles using a 100 kDa MWCO centrifugal filter (Millipore YM-100) to remove the uncoupled peptide.

Further Coupling Reaction with MGB₂ To Achieve the Final Probe. The mAb MGB₂ was conjugated to Fe₃O₄ nanoparticles through an amidation reaction between the amino group of MGB₂ and the carboxyl residue of the peptide attached to the particle surface. The conjugation reaction with mAb MGB₂ was performed at 4 °C. Typically, EDC (10 μmol) and sulfo-NHS (25 μmol) were dissolved in 3 mL of 1 × PBS containing 10 mg of Fe₃O₄ nanoparticles modified with chromophore-labeled peptides. After approximately 15 min, 1 mL of 1 × PBS containing 1.15 mg of mAb MGB₂ was introduced. Typically, the reaction lasted for 10 h. The conjugates were washed several times in 1 × PBS and then stored at 4 °C.

Specific Binding Assays for the Nanoprobes. Fluorescence microscopy and spectroscopy were used to qualitatively evaluate the binding specificity of the nanoprobes to SGC7901 cells and human fibroblast cells. In detail, approximately 1 × 10⁵ SGC7901 and human fibroblast cells were seeded in the wells of two 8-well chamber slides and incubated overnight at 37 °C under 5% CO₂ to allow a firm adherence. After being rinsed with PBS, the cells were incubated with the nanoprobes at 37 °C under 5% CO₂ for 6 h. After that, the cells were rinsed three times with PBS. The fluorescence micrographs were captured using a fluorescence microscope (Olympus X71).

The fluorescence spectra were recorded on a microplate reader (Thermo, Varioskan Flash). In brief, cells were seeded into a 96-well cell culture plate by 1 × 10⁵ cells/well under 100% humidity and incubated overnight at 37 °C under 5% CO₂ to allow a firm adherence. After being rinsed with PBS, the nanoprobes were added at different time points to different wells, and the cells were incubated with the nanoprobes at 37 °C under 5% CO₂. Subsequently, the cells were rinsed three times with PBS, and the fluorescence spectra were recorded.

Animal Tumor Model. The tumor model used was established upon subcutaneous injection of SGC7901 cells (~5 × 10⁶) into male BALB/c nude mice (4–6 weeks old) at the flank region of the right hind leg. The tumor imaging studies were carried out when the tumor size reached 8–10 mm in diameter.

Fluorescence Imaging of Tumors *in Vivo*. The fluorescence images of a nude mouse bearing a subcutaneous tumor at the flank region of the right hind leg were acquired with a Maestro *in vivo* spectrum imaging system (Cambridge Research & Instrumentation, Woburn, MA). Nude mice bearing SGC7901 tumor xenografts were anesthetized, and then the probe was injected into the tumor (10 mg of Fe per kilogram body weight). The excitation filter was a narrow-band filter to allow light with wavelength of 435–480 nm to pass through; the emission filter was a 500 nm long-pass filter. The exposure time for acquiring each fluorescence image was set at 300 ms. The Maestro optical system consists of an optical head that includes a liquid crystal tunable filter (with a bandwidth of 20 nm and a scanning wavelength range of 500–950 nm) with a custom-designed, spectrally optimized lens system that relays the image to a scientific-grade megapixel CCD. The CCD captured the images at each wavelength. The captured images can be analyzed by the vendor software, which uses spectral unmixing algorithms to separate autofluorescence from chromophore signals.

The intensity ratio of fluorescence images captured at 500 and 540 nm, respectively, was then calculated with ImageJ software, based on which pH mapping of the tumor was achieved by converting the I_{500}/I_{540} ratio mapping into pH mapping according to their relationship normalized by taking the absorption of tissue and skin into consideration.

All animal experiments reported herein were performed according to a protocol approved by the Peking University Institutional Animal Care and Use Committee.

Conflict of Interest: The authors declare no competing financial interest.

Acknowledgment. The authors thank the National Basic Research Program of China (2011CB935800), NSFC (21203211, 21321063, 21403250, 81471726), and CAS (CMS-PY-201309, CMS-PY-201314). The authors are grateful to Dr. Liandi Lei from Peking University for her kind help with respect to *in vivo* fluorescence imaging experiments, and to Dr. Xu Cao from Xidian University for quantitative analysis of the ratiometric fluorescence signal. Yi Hou, Jin Zhou, Zhenyu Gao, Xiaoyu Sun, and Chunyan Liu performed the experiments, including synthesis, characterization, and *in vivo* imaging. Dihua Shangguan and Wensheng Yang provided suggestions on the design of the ratiometric dye. Yi Hou and Xiaoyu Sun performed data analysis and wrote the paper. Mingyuan Gao conceived the research, provided guidance, discussed the data, revised and improved the manuscript.

Supporting Information Available: (1) Correction of fluorescence intensity ratio, (2) fluorescence spectra of ANNA and nanoprobe at pH 5.0 and 7.4 under excitation of 455 nm, (3) hydrodynamic size distributions of the final conjugates and the mother particles (Fe₃O₄) determined by DLS method, (4) fluorescence images of SGC7901 cells and human fibroblast cells after being incubated with the nanoprobe, (5) color-coded fluorescence images of normal mouse after subcutaneous injection of the nanoprobe, (6) ratio of fluorescence intensity of ANNA at 500 and 540 nm against pH, and temporal evolutions of pH obtained from corrected ratio of integrated optical intensity in tumor region. This material is available free of charge *via* the Internet at <http://pubs.acs.org>.

REFERENCES AND NOTES

- Farquharson, M. J.; Al-Ebraheem, A.; Falkenberg, G.; Leek, R.; Harris, A. L.; Bradley, D. A. The Distribution of Trace Elements Ca, Fe, Cu and Zn and the Determination of Copper Oxidation State in Breast Tumour Tissue Using μ SRXRF and μ XANES. *Phys. Med. Biol.* **2008**, *53*, 3023–3037.
- Chambers, A. F.; Matrisian, L. M. Changing View of the Role of Matrix Metalloproteinases in Metastasis. *J. Natl. Cancer Inst.* **1997**, *89*, 1260–1270.
- Webb, B. A.; Chimenti, M.; Jacobson, M. P.; Barber, D. L. Dysregulated pH: A Perfect Storm for Cancer Progression. *Nat. Rev. Cancer* **2011**, *11*, 671–677.
- Stearns, M. E.; Wang, M. Type IV Collagenase (M(r) 72,000) Expression in Human Prostate: Benign and Malignant Tissue. *Cancer Res.* **1993**, *53*, 878–883.
- Davies, B.; Waxman, J.; Wasan, H.; Abel, P.; Williams, G.; Krausz, T.; Neal, D.; Thomas, D.; Hanby, A.; Balkwill, F. Levels of Matrix Metalloproteases in Bladder Cancer Correlate with Tumor Grade and Invasion. *Cancer Res.* **1993**, *53*, 5365–5369.
- Moses, M. A.; Wiederschain, D.; Loughlin, K. R.; Zurakowski, D.; Lamb, C. C.; Freeman, M. R. Increased Incidence of Matrix Metalloproteinases in Urine of Cancer Patients. *Cancer Res.* **1998**, *58*, 1395–1399.
- Egeblad, M.; Werb, Z. New Functions for the Matrix Metalloproteinases in Cancer Progression. *Nat. Rev. Cancer* **2002**, *2*, 161–174.
- Gatenby, R. A.; Gawlinski, E. T.; Gmitro, A. F.; Kaylor, B.; Gillies, R. J. Acid-Mediated Tumor Invasion: A Multidisciplinary Study. *Cancer Res.* **2006**, *66*, 5216–5223.

9. Stock, C.; Schwab, A. Protons Make Tumor Cells Move Like Clockwork. *Pflugers Arch.* **2009**, *458*, 981–992.
10. Weissleder, R.; Ntziachristos, V. Shedding Light onto Live Molecular Targets. *Nat. Med.* **2003**, *9*, 123–128.
11. Weissleder, R.; Tung, C. H.; Mahmood, U.; Bogdanov, A. *In Vivo* Imaging of Tumors with Protease-Activated Near-Infrared Fluorescent Probes. *Nat. Biotechnol.* **1999**, *17*, 375–378.
12. Bremer, C.; Tung, C. H.; Weissleder, R. *In Vivo* Molecular Target Assessment of Matrix Metalloproteinase Inhibition. *Nat. Med.* **2001**, *7*, 743–748.
13. McIntyre, J. O.; Fingleton, B.; Wells, K. S.; Piston, D. W.; Lynch, C. C.; Gantam, S.; Matrisian, L. M. Development of a Novel Fluorogenic Proteolytic Beacon for *In Vivo* Detection and Imaging of Tumour-Associated Matrix Metalloproteinase-7 Activity. *Biochem. J.* **2004**, *377*, 617–628.
14. Zhang, Y.; So, M. K.; Rao, J. H. Protease-Modulated Cellular Uptake of Quantum Dots. *Nano Lett.* **2006**, *6*, 1988–1992.
15. Lee, S.; Cha, E. J.; Park, K.; Lee, S. Y.; Hong, J. K.; Sun, I. C.; Kim, S. Y.; Choi, K.; Kwon, I. C.; Kim, K.; et al. A Near-Infrared-Fluorescence-Quenched Gold-Nanoparticle Imaging Probe for *In Vivo* Drug Screening and Protease Activity Determination. *Angew. Chem., Int. Ed.* **2008**, *47*, 2804–2807.
16. Wang, H. W.; Udukala, D. N.; Samarakoon, T. N.; Basel, M. T.; Kalita, M.; Abayaweera, G.; Manawadu, H.; Malalasekera, A.; Robinson, C.; Villanueva, D.; et al. Nanoplatfoms for Highly Sensitive Fluorescence Detection of Cancer-Related Proteases. *Photochem. Photobiol. Sci.* **2014**, *13*, 231–240.
17. Nigam, S.; Barick, K. C.; Bahadur, D. Development of Citrate-Stabilized Fe₃O₄ Nanoparticles: Conjugation and Release of Doxorubicin for Therapeutic Applications. *J. Magn. Magn. Mater.* **2011**, *323*, 237–243.
18. Yu, C. J.; Wu, S. M.; Tseng, W. L. Magnetite Nanoparticle-Induced Fluorescence Quenching of Adenosine Triphosphate-BODIPY Conjugates: Application to Adenosine Triphosphate and Pyrophosphate Sensing. *Anal. Chem.* **2013**, *85*, 8559–8565.
19. Lee, J. H.; Huh, Y. M.; Jun, Y.; Seo, J.; Jang, J.; Song, H. T.; Kim, S.; Cho, E. J.; Yoon, H. G.; Suh, J. S.; Cheon, J. Artificially Engineered Magnetic Nanoparticles for Ultra-sensitive Molecular Imaging. *Nat. Med.* **2007**, *13*, 95–99.
20. Li, Z.; Wei, L.; Gao, M. Y.; Lei, H. One-Pot Reaction To Synthesize Biocompatible Magnetite Nanoparticles. *Adv. Mater.* **2005**, *17*, 1001–1005.
21. Qiao, R. R.; Yang, C. H.; Gao, M. Y. Superparamagnetic Iron Oxide Nanoparticles: From Preparations to *In Vivo* MRI Applications. *J. Mater. Chem.* **2009**, *19*, 6274–6293.
22. Zeng, J. F.; Jing, L. H.; Hou, Y.; Jiao, M. X.; Qiao, R. R.; Jia, Q. J.; Liu, C. Y.; Fang, F.; Lei, H.; Gao, M. Y. Anchoring Group Effects of Surface Ligand on Magnetic Properties of Fe₃O₄ Nanoparticles: Towards High Performance MRI Contrast Agents. *Adv. Mater.* **2014**, *26*, 2694–2698.
23. Zhou, J.; Fang, C. L.; Chang, T. J.; Shangguan, D. H. A pH Sensitive Ratiometric Fluorophore and Its Application for Monitoring the Intracellular and Extracellular pHs Simultaneously. *J. Mater. Chem. B* **2013**, *1*, 661–667.
24. Han, J. Y.; Loudet, A.; Barhoumi, R.; Burghardt, R. C.; Burgess, K. A Ratiometric pH Reporter for Imaging Protein–Dye Conjugates in Living Cells. *J. Am. Chem. Soc.* **2009**, *131*, 1642–1643.
25. Albertazzi, L.; Storti, B.; Marchetti, L.; Beltram, F. Delivery and Subcellular Targeting of Dendrimer-Based Fluorescent pH Sensors in Living Cells. *J. Am. Chem. Soc.* **2010**, *132*, 18158–18167.
26. Doussineau, T.; Smahi, M.; Mohr, G. J. Two-Dye Core/Shell Zeolite Nanoparticles: A New Tool for Ratiometric pH Measurements. *Adv. Funct. Mater.* **2009**, *19*, 117–122.
27. Snee, P. T.; Somers, R. C.; Nair, G.; Zimmer, J. P.; Bawendi, M. G.; Nocera, D. G. A Ratiometric CdSe/ZnS Nanocrystal pH Sensor. *J. Am. Chem. Soc.* **2006**, *128*, 13320–13321.
28. Hu, X. G.; Gao, X. H. Silica-Polymer Dual Layer-Encapsulated Quantum Dots with Remarkable Stability. *ACS Nano* **2010**, *4*, 6080–6086.
29. Jin, T.; Sasaki, A.; Kinjo, M.; Miyazaki, J. A Quantum Dot-Based Ratiometric pH Sensor. *Chem. Commun.* **2010**, *46*, 2408–2410.
30. Park, J.; An, K. J.; Hwang, Y. S.; Park, J. G.; Noh, H. J.; Kim, J. Y.; Park, J. H.; Hwang, N. M.; Hyeon, T. Ultra-Large-Scale Syntheses of Monodisperse Nanocrystals. *Nat. Mater.* **2004**, *3*, 891–895.
31. Hou, Y.; Qiao, R. R.; Fang, F.; Wang, X. X.; Dong, C. Y.; Liu, K.; Liu, C. Y.; Liu, Z. F.; Lei, H.; Wang, F.; et al. NaGdF₄ Nanoparticle-Based Molecular Probes for Magnetic Resonance Imaging of Intraperitoneal Tumor Xenografts *In Vivo*. *ACS Nano* **2013**, *7*, 330–338.
32. Majonis, D.; Herrera, I.; Ornaty, O.; Schulze, M.; Lou, X. D.; Soleimani, M.; Nitz, M.; Winnik, M. A. Synthesis of a Functional Metal-Chelating Polymer and Steps toward Quantitative Mass Cytometry Bioassays. *Anal. Chem.* **2010**, *82*, 8961–8969.
33. Zhang, F. M.; Ren, G.; Lu, Y. Y.; Jin, B.; Wang, J.; Chen, X.; Liu, Z. X.; Li, K.; Nie, Y. Z.; Wang, X.; et al. Identification of TRAK1 (Trafficking Protein, Kinesin-Binding 1) as MGb₂-Ag: A Novel Cancer Biomarker. *Cancer Lett.* **2009**, *274*, 250–258.
34. Zheng, H. C.; Takahashi, H.; Murai, Y.; Cui, Z. G.; Nomoto, K.; Niwa, H.; Tsuneyama, K.; Takana, Y. Aberrant Pim-3 Expression Is Involved in Gastric Adenoma-Adenocarcinoma Sequence and Cancer Progression. *Anticancer Res.* **2006**, *26*, 3579–3584.
35. Pillay, C. S.; Elliott, E.; Dnnison, C. Endolysosomal Proteolysis and Its Regulation. *Biochem. J.* **2002**, *363*, 417–429.